atoms

MDPI

Article

An Analytical Model for the Time Distribution of Muonic Oxygen X-Rays in Muonic Experiments

Petar Danev [1,*], Iavor Boradjiev [1,2,*] and Hristo Tonchev [1]

[1] Institute for Nuclear Research and Nuclear Energy, Bulgarian Academy of Sciences, Blvd. Tsarigradsko ch. 72, 1784 Sofia, Bulgaria
[2] Faculty of Hydraulic Engineering, University of Architecture, Civil Engineering and Geodesy, 1 Hristo Smirnenski Blvd., 1046 Sofia, Bulgaria
* Correspondence: petar_danev@abv.bg (P.D.); borajiev@inrne.bas.bg (I.B.)

Abstract

We propose an analytical model and perform numerical simulations to study the time distribution of the characteristic muonic oxygen X-ray emission following muon transfer from muonic hydrogen to oxygen in a $H_2 + O_2$ gas mixture. The model accounts for all fundamental processes that alter the kinetic energy and spin distribution of muonic hydrogen atoms. The impact of the uncertainties in various experimental parameters on the precision of the computed results is studied in detail by means of the Monte Carlo method. Specifically, we observe the presence of a minimum in the time dependence of the relative standard deviation of X-ray emission for realistic parameter combinations, which can serve as a benchmark for comparing experiments and numerical simulations. Verification against available experimental data reveals the potential of this approach for both description and parameter optimization in the planning and analysis of muonic experiments

Keywords: exotic atoms; numerical simulations; uncertainty propagation

1. Introduction

Spectroscopy of light atomic systems provides data of exceptionally high precision, enabling the refinement of fundamental physical constants [1,2]. Exotic systems such as muonic hydrogen and muonic deuterium offer a unique opportunity to further enhance the experimental accuracy of such measurements. This has been exemplified by the determination of the proton charge radius through measurement of the Lamb shift in muonic hydrogen [3].

Another quantity of fundamental importance is the Zemach radius of the proton, R_Z, which characterizes the combined spatial distributions of the proton's charge and its magnetic dipole moment. Its precise determination is important not only for a deeper understanding of the fundamental structure of the proton but also because it serves as a limiting factor in testing the accuracy of modern high-precision quantum electrodynamics calculations. Previous extractions of R_Z from hyperfine-splitting measurements in ordinary and muonic hydrogen yielded values of $R_Z = (1.037 \pm 0.016)$ fm [4], $R_Z = (1.045 \pm 0.016)$ fm [5], and $R_Z = (1.082 \pm 0.037)$ fm [6]. A more recent lattice-QCD study [7] reported $R_Z = (1.013 \pm 0.010_{\text{stat}} \pm 0.012_{\text{syst}})$ fm, while an updated analysis, incorporating new spin-structure constraints, yielded $R_Z = (1.036 \pm 0.008)$ fm [8]. In parallel, high-resolution spectroscopy experiments aiming to determine the hyperfine splitting of the ground state of muonic hydrogen—such as those conducted by the CREMA [9] and

Check for updates

Received: 17 February 2026
Revised: 2 April 2026
Accepted: 23 April 2026
Published: 27 April 2026

Copyright: © 2026 by the authors. Licensee MDPI, Basel, Switzerland. This article is an open access article distributed under the terms and conditions of the Creative Commons Attribution (CC BY) license.

FAMU [10] collaborations—are expected to further reduce the experimental uncertainty of R_Z.

A central aspect of all these experiments is the muon transfer from muonic hydrogen to a heavier element, followed by a relaxation of the muon to the ground state, possibly accompanied by emission of characteristic X-rays. These X-rays serve as the primary observable in experiments and provide indirect information for the muon transfer dynamics. Precise modeling of the muon transfer process, including its energy dependence, background contributions, and sensitivity to experimental conditions, is essential for interpreting the experimental results. Several studies have addressed this topic, for example, the muon transition from muonic hydrogen to oxygen and sulfur molecules, which has been investigated in [11,12]. In these studies, a simple model expression for the collision energy-dependent muon transition rate to oxygen has been obtained by fitting to experimental data. However, recently, Stoilov et al. [13] derived a more precise expression for this quantity under specific assumptions, building on the results of the FAMU collaboration [14]. A comprehensive description must also include the interaction of muonic hydrogen with the surrounding atoms and molecules. The relevant cross-sections and rates of elastic and inelastic scattering of $p\mu$ on hydrogen molecules, including the spin structure of $p\mu$, have already been provided by A. Adamczak in [15].

Muonic spectroscopy experiments are inherently complex, and achieving the required precision in the directly measured quantity demands a detailed understanding of all underlying atomic and molecular processes. Consequently, realistic simulations of these processes play a crucial role both in the design and in the analysis of muonic experiments.

In this work, we present an analytical model that describes the time evolution of an ensemble of muonic hydrogen atoms in a gas mixture of H_2 + O_2, including the process of muon transfer to oxygen. The model accounts for the key physical processes affecting the energy and spin distributions of muonic hydrogen atoms. We analyze the influence of uncertainties in the model parameters and approximations using a Monte Carlo approach and perform time-dependent simulations to study the propagation of these uncertainties. Our simulations reveal the existence of a "minimum-uncertainty time", at which the relative uncertainty of the muonic X-ray emission reaches a minimum—providing a useful benchmark for optimizing experimental timing and precision. The simulated results are compared with experimental data from [11], showing good agreement and indicating possible refinements in the current muon transfer parameters. The proposed model provides a flexible and transparent framework for simulating muonic processes and assessing their precision. It can be readily adapted to support the planning and optimization of future muonic hydrogen spectroscopy experiments. While similar models for muon transfer have been employed by the FAMU [16] and CREMA [17] collaborations, the present approach is formulated independently of any specific experimental setup, making it broadly applicable to the study of muonic systems.

This paper is organized as follows: In Section 2, we review the analytical model. The model parameters and the approximations used are discussed in Section 3. In Section 4, we introduce estimators that quantify both the average behavior and the precision of our simulations. The main numerical results concerning the simulation precision are presented and discussed in Section 6. The model's ability to provide a rigorous description of muon transfer experiments is assessed in Section 7. A comparison with the experimental data is provided in Section 8, and the conclusions are outlined in Section 9.

2. Muonic Hydrogen Decay Model

Modeling the time evolution of muonic hydrogen atoms in a gas mixture is a complex task due to the variety of processes that contribute to the change in the number and state of

these atoms. In this section, we present an analytical model to describe the time, energy, and spin distribution of the $p\mu$ atoms in a gaseous mixture of hydrogen and oxygen molecules. A key aspect of this investigation is determining the time evolution of the rate of muon transfer from hydrogen to oxygen in the gas. This quantity is essential for interpreting the experimentally accumulated data [10,11].

In our model, the state of a muonic hydrogen atom is described by two quantities—its kinetic energy and the total spin of the system. In the ground state of $p\mu$, the hydrogen nucleus and the muon spins can be coupled into singlet and triplet states, which will be denoted by $F_\alpha = 0, 1$, respectively. To simplify the problem, we discretize the kinetic energy into n bins, denoted as E_i for $i = 1, \ldots, n$. The state of $p\mu$ is then represented as a $2n$-dimensional vector $N_{(i\alpha)}(t) = N(E_i, F_\alpha, t)$, whose time evolution is governed by the relation

$$N(t) = \mathrm{e}^{Lt}\, N(0), \tag{1}$$

where the vector $N(0)$ represents the initial distribution of $p\mu$ atoms, and the (i, α)-th component of the vector $N(t)$ gives the probability of finding a $p\mu$ atom with energy E_i and spin $F = \alpha$ at time t. The $2n \times 2n$ matrix L encapsulates the contributions from various processes affecting the $p\mu$ state. For simplicity, L is divided into two components—a diagonal matrix L_d and a dense matrix L_s—such that $L = L_d + L_s$.

The matrix L_d accounts for processes such as muon decay and nuclear capture rates, represented by λ_0, and the formation rates of muonic oxygen ($O\mu$), muonic deuterium ($d\mu$), and molecular ions ($pp\mu$) through the corresponding rates $\Lambda_{pO} = \mathrm{diag}\{\lambda^0_{pO}, \lambda^1_{pO}\}$, $\lambda_{d\mu}$, and $\lambda_{pp\mu}$. Explicitly, L_d is given by

$$L_d = -\left(\lambda_0\, I_{2n} + \phi(c_p \lambda_{pp\mu}\, I_{2n} + c_d \lambda_{d\mu}\, I_{2n} + c_O\, \Lambda_{pO})\right). \tag{2}$$

where I_{2n} is the $2n \times 2n$ identity matrix, ϕ is the number density of the atoms of the gas mixture in LHD units, and c_p, c_d, and c_O are the number concentrations of hydrogen, deuterium, and oxygen atoms, respectively. The n-dimensional vectors $\lambda^\alpha_{pO}\,(\alpha = 0, 1)$ correspond to the energy-dependent muon transfer rate from muonic hydrogen with spin $F = \alpha$ hydrogen to oxygen. All transition rates except λ_0 are normalized to the liquid hydrogen density $N_{LHD} = 4.25 \times 10^{22}$ atoms/cm^3.

The transition matrix L_s describes the elastic and inelastic scattering of muonic hydrogen by hydrogen molecules in the gas mixture:

$$L_s = \phi c_p \begin{bmatrix} \lambda^{00,T} - \mathrm{diag}\{\mathcal{I}_n^T \cdot (\lambda^{00} + \lambda^{01})\} & \lambda^{10,T} \\ \lambda^{01,T} & \lambda^{11,T} - \mathrm{diag}\{\mathcal{I}_n^T \cdot (\lambda^{10} + \lambda^{11})\} \end{bmatrix} \tag{3}$$

Here, $\mathcal{I}_n$ is an n-dimensional column vector of ones, and $\lambda^{\alpha\beta}(\,\alpha, \beta = 0, 1)$ are $n \times n$ matrices comprising $p\mu$ scattering rates on hydrogen. Specifically, $\lambda^{\alpha\beta}_{ij}$ denotes the transition rate of a $p\mu$ atom from a quantum state with spin $F = \alpha$ and kinetic energy E_i to a state with $F = \beta$ and E_j.

In summary, solving the full continuous system of ODEs to find the muonic hydrogen evaluation is too costly, being both more time-consuming and potentially less accurate. Instead, after discretization, we compute the matrix exponential $\exp(\Delta t\, L)$ once, and subsequently obtain the exact (point-wise) time evolution through iterative multiplication by this matrix exponential. Matrix multiplication is a numerically stable operation, highly parallelizable, and computationally efficient.

The primary quantity of interest is the transfer rate from hydrogen to oxygen in the gas, expressed as the number of transfers from hydrogen to oxygen per unit time:

$$\frac{\mathrm{d}N_{p\mu\to O\mu}}{\mathrm{d}t}(t) = \phi c_O \mathcal{I}_{2n}^{T} \cdot \Lambda_{pO} \cdot N(t). \tag{4}$$

The emitted characteristic X-rays following the muon transfer to oxygen occur on a timescale much shorter ($\sim 10^{-13}$ s [18]) than other simulated processes ($\sim 10^{-6} - 10^{-10}$ s). Therefore, we can approximate the experimentally measurable X-ray emission rate as directly proportional to the muon transfer rate to oxygen in the gas. In the subsequent discussion, we will consider these two rates as equivalent:

$$\mathrm{d}N_O/\mathrm{d}t \equiv \mathrm{d}N_{p\mu\to O\mu}/\mathrm{d}t. \tag{5}$$

3. Model Parameters and Sources of Errors

Constructing a realistic model for the muon transfer rate requires accounting for a large number of physical processes, each characterized by its own set of parameters known with varying degrees of precision. For some of these processes, limited or no experimental data are available. In addition, the numerical methods employed for the simulation of the model have inherent advantages and limitations, which necessitate the use of several assumptions and approximations.

In this section, we classify the different groups of parameters and sources of uncertainty, and analyze the impact of the approximations introduced. In some cases (e.g., numerical accuracy, time and energy discretization, $p\mu$ scattering rates), we assess their influence on the simulation results and argue that it is negligible. In others (e.g., the initial distribution of muonic hydrogen atoms, the muon transfer rate to oxygen $\lambda_{pO}(E)$), further investigation (presented in the following sections) is required.

3.1. Physical Constants

In our computations, we use the most recent values of the physical constants necessary to calculate the muon decay rate according to the presented model. These are provided in Table 1.

Table 1. Physical constants used in the model.

Quantity	Label	Value	Ref.
Total muon decay rate	λ_0	$(4.66501 \pm 0.00014) \times 10^5\ \mathrm{s}^{-1}$	[19]
$pp\mu$ formation rate	$\lambda_{pp\mu}$	$(2.01 \pm 0.07) \times 10^6\ \mathrm{s}^{-1}$	[20]
$d\mu$ formation rate	$\lambda_{d\mu}$	$(1.64 \pm 0.16) \times 10^{10}\ \mathrm{s}^{-1}$	[16]
Muonic hydrogen mass	$\mathrm{m}_{p\mu}$	$(1043.927647 \pm 0.000023) \times 10^6\ \mathrm{eV/c}^2$	[21]
Oxygen molecule mass	m_{O_2}	$(29806 \pm 2) \times 10^6\ \mathrm{eV/c}^2$	[21]

3.2. Experimentally Controllable Quantities

Some of the model parameters depend on the specific conditions of a particular experiment. In order to maintain a certain level of concreteness, we focus on the physical variables' values used in the measurements reported by Werthmüller et al. [11]. These values are summarized in Table 2. By using parameter values corresponding to a real experiment, we can compare the predictions of our model with the experimentally observed data provided in [11].

Table 2. Experimental parameter values.

Quantity	Label	Value	Ref.
Oxygen atom concentration	c_O	$(39.60 \pm 0.40) \times 10^{-4}$	[11]
Deuterium nuclei concentration	c_d	$(1.50 \pm 0.05)(1 - c_O) \times 10^{-4}$	[11]
Temperature	T	(297.15 ± 0.50) K	[11]
Pressure	P	(15.06 ± 0.05) bar	[11]

3.3. Number Density of Atoms ϕ

To calculate the number density of atoms normalized to LHD, ϕ in Equation (2), we have adopted the ideal gas approximation. This simplifies ϕ to a function of the pressure and temperature ratio: $\phi(P/T) = P/(k_B T N_0) \approx 0.3408 \times P/T$, where P is in units of bars. Since the hydrogen constitutes the predominant portion of the gas mixture, and at the temperature of interest only a small portion of the gas particles engage in inelastic scattering processes, this approximation is sufficiently accurate for our study. For the set of experimental parameters used in our simulations, the deviations due to this approximation remain within 1% [22].

In our analysis, the uncertainties in the number of muon events stemming from ϕ are effectively accounted for through the uncertainties in temperature and pressure.

3.4. Initial Distribution of Muonic Hydrogen

It is known that the initial kinetic energy distribution of the muonic hydrogen, $N(0)$, does not conform to a simple Maxwellian profile. Experimental and theoretical studies suggest the existence of a high-energy $p\mu$ population [11,23]. Therefore, for $p\mu$ atoms in both singlet and triplet spin states, we adopt the "two-component model", proposed in [11], where a fraction κ of $p\mu$ atoms resides at an initial energy E_0^{high} of approximately 20 eV and the remaining fraction $(1 - \kappa)$ follows Maxwell statistics. In our simulations, we use $\kappa = 0.4 \pm 0.1$, which approximates the results presented in [23] for the corresponding experimental parameters. We also assume that, at the onset of the process, the muonic hydrogen atoms are statistically distributed between the two hyperfine spin states: $1/4$ in the singlet state ($F = 0$) and $3/4$ in the triplet state ($F = 1$).

To account for the uncertainty in the position of the high-energy component in the initial $p\mu$ distribution, we introduce an uncertainty in E_0^{high} as $E_0^{\text{high}} = \bar{E}_0^{\text{high}} \pm \Delta E_0^{\text{high}}$, where $\bar{E}_0^{\text{high}} = 20$ eV and $\Delta E_0^{\text{high}} = 2$ eV, approximately matching the width of an energy bin.

3.5. Numerical Accuracy and Time Discretization

We verify that in computing the muon transfer rate, the numerical errors are several orders of magnitude smaller than the uncertainties introduced by the approximations and experimental parameter uncertainties discussed earlier. Consequently, these numerical errors can be considered negligible in our analysis.

We compute the time evolution of the muonic hydrogen distribution using discrete time steps. Since the matrix L governing this evolution is time-independent, this discretization does not introduce any errors. Therefore, the errors in the muon transfer rate arise solely from the accumulation of the numerical error during the evolutionary steps. Given the high precision of the numerical methods used, the numerical errors inherent in these approaches are minimal and do not significantly impact the overall accuracy and precision of the results.

3.6. $p\mu$ Atom Kinetic Energy Discretization

From Equations (1) and (4), it is evident that the errors due to the muon hydrogen kinetic energy discretization can be effectively incorporated into the uncertainties of the energy-dependent quantities—muonic hydrogen scattering rates, the transfer rate of muons to oxygen, and the initial distribution. When these discretization errors are smaller than the respective uncertainties, as is the case in the regime considered here, they do not significantly affect the precision of the simulation.

3.7. Muonic Hydrogen Scattering Rates $\lambda^{\alpha,\beta}$

The elastic and inelastic scattering rates of muonic hydrogen, $\lambda_{ij}^{\alpha,\beta}$ $(\alpha, \beta = 0, 1)$, at a temperature of $T = 300$ K, used in our simulations, are taken from Adamczak (private communications). They have been calculated using the theoretical framework and numerical procedures described in [15], where differential cross-sections for muonic atom scattering from hydrogen molecules are computed. These rates, not available in tabulated form in the literature, are averaged over the Boltzmann distribution of the initial rotational levels of the H_2 molecule and over the Maxwellian kinetic energies of these molecules, for the given gas temperature. Furthermore, a downward spin-flip transition $F = 1 \to F = 0$ is given for a single averaged value of the projection F_z of the initial total spin $F = 1$. $\lambda^{\alpha,\beta}$ are computed with a relative uncertainty of $\sigma^{\lambda_{ij}^{\alpha,\beta}}/\mu^{\lambda_{ij}^{\alpha,\beta}} \lesssim 10^{-5}$ and an absolute uncertainty $\sigma^{\lambda_{ij}^{\alpha,\beta}} \lesssim 10^5\ \mathrm{s}^{-1}$ up to 100 eV, ensuring that their uncertainty can be safely neglected.

3.8. Transfer Rate of Muons from $p\mu$ to Oxygen $\lambda_{pO}(E)$

The collision energy-dependent transfer rate of muons from hydrogen in a singlet state to oxygen $\lambda_{pO}^{0s}(E^c)$ is a key quantity for studying the time evolution of muon transfer to oxygen. Only recently was $\lambda_{pO}^{0s}(E^c)$ obtained with sufficient accuracy [13], thus enabling more precise simulations of such physical processes.

To obtain the $p\mu$ kinetic energy-dependent transfer rate with respect to the laboratory reference frame, $\lambda_{pO}^{0}(E, T)$, we proceed as follows: First, we express the collision energy in terms of the solid angle Ω between the momenta of the $p\mu$ atom and the (point) O_2 molecule, and their kinetic energies E and E_{O_2} correspondingly. Then, we average $\lambda_{pO}^{0s}(E^c(E, E_{O_2}, \Omega))$ over the kinetic energy of the oxygen molecule E_{O_2} and the solid angle Ω, weighted with the Maxwell distribution $f_M(T, E)$ for temperature T,

$$\lambda_{pO}^{0}(E, T) = \int_0^\infty \int_\Omega f_M(T, E^c)\lambda_{pO}^{0s}(E^c)\frac{\mathrm{d}\Omega}{4\pi}\mathrm{d}E_{O_2}. \tag{6}$$

The use of Maxwell distribution of O_2 atoms in the gas is just an approximation, since the gas is a mixture of real gases. The associated uncertainty is assumed to be incorporated into the uncertainty of $\lambda_{pO}^{0s}(E^c)$ (obtained under the assumption of Maxwell distribution over E^c). Moreover, during the first tens of nanoseconds until thermalization occurs, the O_2 distribution is time-dependent; however, in the subsequent discussions, this time dependence will be neglected. The uncertainty of $\lambda_{pO}^{0s}(E^c)$ is propagated into the uncertainty of $\lambda_{pO}(E, T)$ through Equation (6).

The energy dependence of the muon transfer rate $\lambda_{pO}(E)$ used in our simulations is characterized by relatively small uncertainties for $p\mu$ energies up to $E \simeq 0.1$ eV [13]. For higher energies ($E \gtrsim 0.1$ eV), however, the values of $\lambda_{pO}(E)$ are known with lower precision. To address this, we consider two scenarios: a moderate one, where a smooth extrapolation of $\lambda_{pO}(E)$ uncertainty is applied, and a conservative scenario, where for $E > 0.1$ eV, the uncertainty is assumed to be significantly larger. In our simulations, we use the energy dependence of the muon transfer rate $\lambda_{pO}(E)$ as given in [13] in parametric

form. It is characterized by relatively small uncertainties for $p\mu$ energies up to $E \simeq 0.1$ eV. For higher energies ($E \gtrsim 0.1$ eV), however, the values of $\lambda_{pO}(E)$ are not well constrained, and the associated uncertainty is not specified in [13]. To account for this, we consider two extreme scenarios that bracket the plausible range of $\lambda_{pO}(E)$: a moderate scenario, in which the uncertainty for $E < 0.1$ eV is smoothly extrapolated to higher energies, and a conservative scenario, in which the uncertainty for $E > 0.1$ eV is assumed to be significantly larger; see Figure 1a,b.

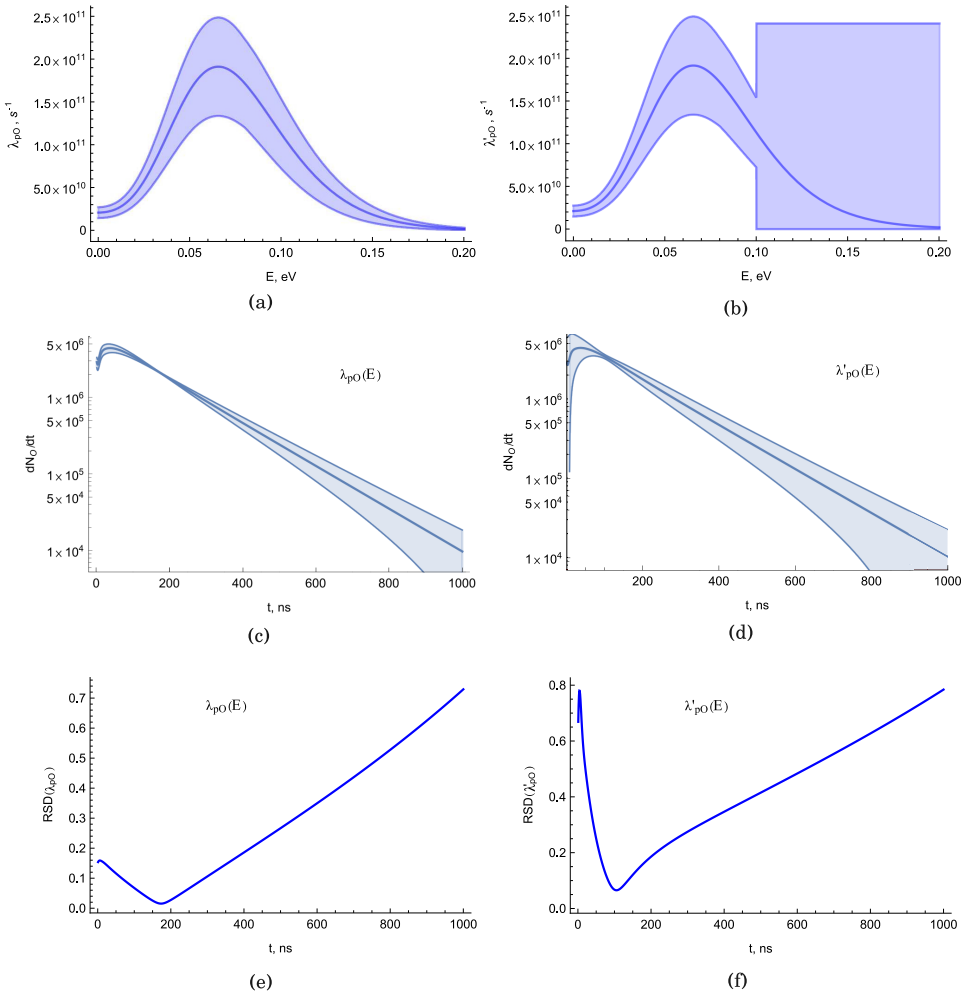


Figure 1. The energy dependence of the muon transfer rate $\lambda_{pO}(E)$, along with its 95% confidence interval, is displayed in the top panels. For $E \leq 0.1$ eV, the confidence interval is taken from [13], while for $E > 0.1$ eV, two scenarios are considered: moderate (**a**) and conservative (**b**). The corresponding muon transfer rate dN_O/dt and relative standard deviation $RSD(\lambda_{pO})$ computed with the respective $\lambda_{pO}(E)$ are presented in the middle and bottom rows (panels (**c**), (**d**) and (**e**), (**f**), respectively). The muon transfer rate is plotted on a logarithmic scale.

The conservative uncertainty has been chosen "ad hoc" in order to ensure better compatibility with the experimental data reported in Ref. [11]. At the same time, the imposed upper limit was selected such that it remains physically consistent with theoretical studies showing that $\lambda_{pO}(E)$ decreases at higher collision energies [24]. The resulting estimate can be regarded as a conservative uncertainty, as it likely overestimates the true uncertainty of $\lambda_{pO}(E \gg 0.1$ eV). Nevertheless, this has no practical consequence for the low-energy muonic experiments considered here, since the fraction of high-energy muonic hydrogen atoms is negligible and does not influence the experimental outcomes. The 95% confidence intervals for both cases are shown in the upper panels of Figure 1.

To the best of our knowledge, there are no experimental measurements of the muon transfer rate from the triplet state ($F = 1$) of muonic hydrogen to oxygen $\lambda^1_{pO}(E)$. Therefore, we assume that $\lambda^1_{pO}(E)$ is equal to the transfer rate from the singlet state, i.e., $\lambda^1_{pO}(E) = \lambda^0_{pO}(E) \equiv \lambda_{pO}(E)$. This approximation may introduce minor deviations from the actual time dependence of the muon transfer rate only in the first few tens of nanoseconds, prior to the thermalization of the gas. However, its impact is negligible at later times, as the $p\mu$ atoms in the excited state rapidly converge to their spin ground state ($F = 0$).

4. Estimators: Sample Mean, Sample Standard Deviation, and Sample Relative Standard Deviation

The time interval of 1 μs is divided into 1000 time slices of size $\Delta t_{j+1} = t_{j+1} - t_j = 1$ ns, where $j = 0, 1, \ldots, 1000$. For each parameter X presented in Section 3, and at each time t_j, we conducted a large number of Monte Carlo simulation runs ($N_{\text{run}} = 1000$), evaluating the respective muon transfer rates to oxygen, $(\mathrm{d}N_O/\mathrm{d}t(x_i; t_j))$, with $1 \leq i \leq N_{\text{run}}$. For each run, a random value x_i of the parameter X was selected, based on the distribution of its uncertainty, while all other quantities were kept at their mean values. Finally, for the $(j+1)^{\text{th}}$ time bin, the relative standard deviation (RSD) of $(\mathrm{d}N_O/\mathrm{d}t(x_i; t_j))$ due to uncertainties in X is computed as

$$RSD^{\mathrm{d}N_O/\mathrm{d}t}(X; t_j) = \frac{\sigma^{\mathrm{d}N_O/\mathrm{d}t}(X; t_j)}{\mu^{\mathrm{d}N_O/\mathrm{d}t}(X; t_j)}, \tag{7}$$

where the mean and standard deviation of the muon transfer rate are defined as

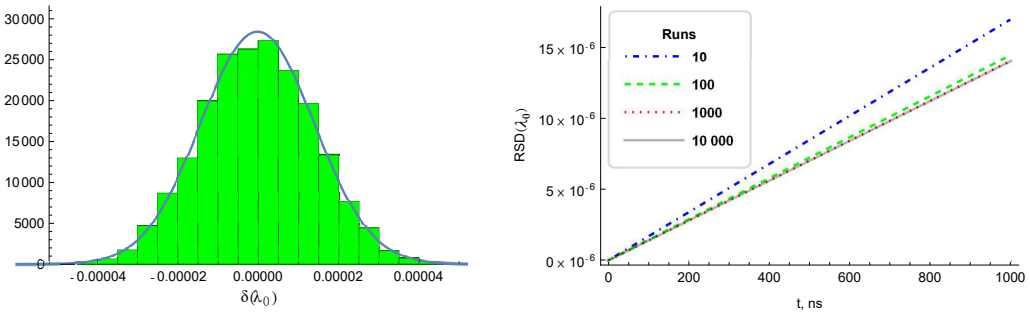
$$\mu^{\mathrm{d}N_O/\mathrm{d}t}(X; t_j) = \frac{1}{N_{\text{run}}} \sum_{i=1}^{N_{\text{run}}} \frac{\mathrm{d}N_O}{\mathrm{d}t}(x_i; t_j), \tag{8}$$

$$\sigma^{\mathrm{d}N_O/\mathrm{d}t}(X; t_j) = \sqrt{\frac{1}{N_{\text{run}} - 1} \sum_{i=1}^{N_{\text{run}}} \left(\frac{\mathrm{d}N_O}{\mathrm{d}t}(x_i; t_j) - \mu^{\mathrm{d}N_O/\mathrm{d}t}(X; t_j) \right)^2}. \tag{9}$$

Since we are primarily interested in the impact of the parameter X's uncertainty on the time distribution of the muon transfer rate from hydrogen to oxygen $\mathrm{d}N_O/\mathrm{d}t$, in the following text, we adopt a simplified notation $RSD^{\mathrm{d}N_O/\mathrm{d}t}(X; t_j) \equiv RSD(X)$ and $\mu^{\mathrm{d}N_O/\mathrm{d}t}(X; t_j) \equiv \mu(X)$. If necessary, the time variable t_j will be explicitly indicated.

Two remarks are in order. First, our simulations show that relatively small uncertainties in the normally distributed parameters lead to uncertainties in the muon transfer events $\mathrm{d}N_O/\mathrm{d}t(t)$ that follow a distribution very close to normal. This is illustrated in Figure 2a, which presents a histogram of the relative uncertainty in $\mathrm{d}N_O/\mathrm{d}t(t = 1000$ ns), caused by the uncertainty in λ_0, for 10,000 runs. The solid curve represents a normal distribution with the same mean and standard deviation.

Second, to demonstrate that the chosen number of simulation runs is optimal for our investigation, we performed simulations with different values of N_{run} and plotted the results in Figure 2b. The curves corresponding to $N_{\text{run}} = 1000$ and $N_{\text{run}} = 10,000$ are visually indistinguishable.



(a) (b)

Figure 2. (**a**) Distribution of the relative deviation of the muon transfer rate to oxygen, $\delta(\lambda_{0i}) = [\mathrm{d}N_O^{\lambda_0}/\mathrm{d}t(\lambda_{0i}) - \mathrm{d}N_O^{\lambda_0}/\mathrm{d}t(\mu(\lambda_0))]/[\mathrm{d}N_O^{\lambda_0}/\mathrm{d}t(\mu(\lambda_0))]$, at $t = 1000$ ns, caused by the uncertainty in λ_0, for $N_{\mathrm{run}} = 10,000$. The solid line represents the corresponding normal distribution. (**b**) Relative standard deviation of $\mathrm{d}N_O/\mathrm{d}t$ resulting from the uncertainties in λ_0, calculated for a selected number of simulation runs.

5. Sampling the Parameter Space

We assume that all quantities are statistically independent. This is clearly valid for the molecular concentrations, the muon hydrogen scattering rates, and the intrinsic properties such as masses. Regarding the temperature T, pressure P, and muon transfer rate to oxygen λ_{pO}, we make the following proviso: We consider only the uncertainties in the initially measured values of P and T, as well as the corresponding uncertainty of the muon transfer rate $\lambda_{pO}(E,T)$. Possible temporal shifts and fluctuations of P and T and cross-correlations, arising from the interdependence of P and T through the equation of state, and between T and $\lambda_{pO}(E,T)$ via (6), are not taken into account.

Consequently, instead of analyzing all parameter uncertainties simultaneously, it is sufficient to perform one-at-a-time parameter sweeps, while keeping all the remaining parameters fixed. This approach is supported by the analytical considerations in Section 6.5, where the leading contributions in the series expansion of the RSD^2 arise from terms linear in the individual variances $(\sigma^{X_k})^2$. In this way, we can easily identify the dominant sources of uncertainties, and densely traverse their respective parameter spaces.

Furthermore, we have conducted simulations by sampling both the full parameter space and a reduced space limited to the parameters contributing the largest uncertainties. Comparing these results, we confirm the validity of the reduced-parameter approximation within the investigated regime.

6. Propagation of Uncertainty in the Muon Transfer Rate: *RSD* Dynamics

In this section, we present the results of numerical simulations showing the impact of the uncertainties in a single physical variable on the precision of the simulated muon transfer rate to oxygen $\mathrm{d}N_O/\mathrm{d}t$. We consider a time interval of 1 μs since this is approximately the time span of the most informative experimental observation.

6.1. Uncertainties in the Physical Constants

The impact of the uncertainties of the physical constants used in the simulations on the time distribution of the relative standard deviation of the muon transfer rate is shown in Figure 3. The *RSD* values due to the quantities listed in Table 1 range from less than 1% (for $\lambda_{pp\mu}$, $\lambda_{d\mu}$) to significantly lower values for other constants.

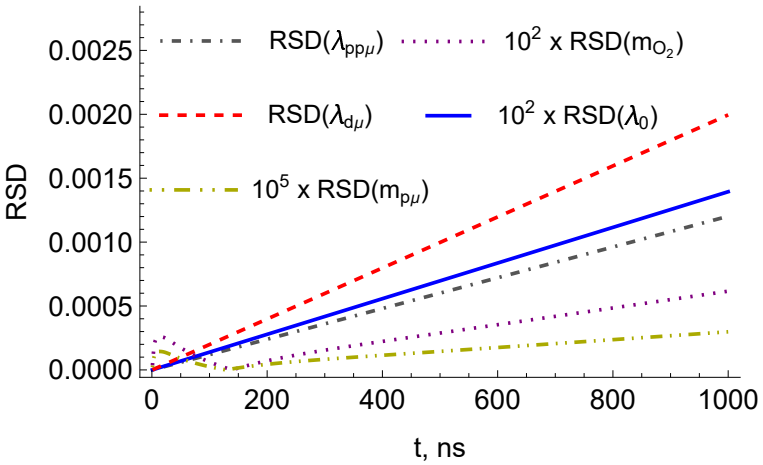


Figure 3. Relative standard deviation of the muon transfer rate determined by uncertainties in various physical constants used in the simulations, plotted as a function of time.

6.2. Uncertainties in the Controllable Experimental Parameters

Unlike the physical constants, the other parameters used in the simulations depend heavily on the conditions of the modeled experiment. In this study, we utilized the mean values and the uncertainties of the controllable parameters corresponding to the experiment described in [11] (given in Table 2) to verify the results of our simulations. As shown in Figure 4, the *RSD* of the muon transfer events due to inaccuracies in the experimentally controlled parameters P, T, c_O, and c_d is significantly higher than that resulting from the uncertainties in the physical constants. As discussed in Section 6.6, the effect of the uncertainties in these parameters on the experimentally observed data in precise muonic experiments can be estimated.

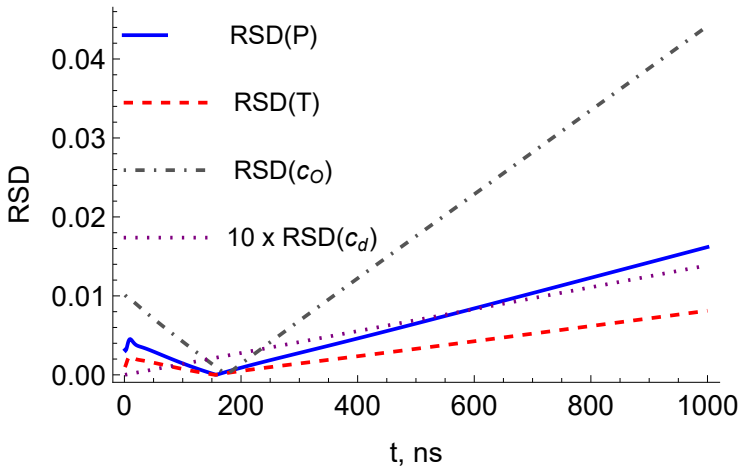


Figure 4. Relative standard deviation of the muon transfer rate determined by uncertainties in the experimentally controlled parameters in the model, plotted as a function of time.

6.3. Uncertainty in the Initial Condition

The relative standard deviation in the muon transfer rate to oxygen, arising from the assumptions regarding the initial state of $p\mu$ atoms as discussed in Section 3.4, is shown in Figure 5. The uncertainties in the fraction of the high-energy component κ and its mean energy $\bar{E}^{\text{high}}$ (both with normal distribution and standard deviations, respectively σ^{κ} and $\sigma^{\bar{E}^{\text{high}}}$) result in significant variations in dN_O/dt at the first moments after the formation of $p\mu$ atoms. As expected, the initial energy distribution has a major impact during the thermalization phase of $p\mu$ atoms, while its influence diminishes significantly—by approximately a factor of 20—once thermalization is complete. The figure demonstrates that

RSD due to uncertainties in the high-energy component fraction is an order of magnitude larger than that caused by its mean energy for the chosen uncertainties.

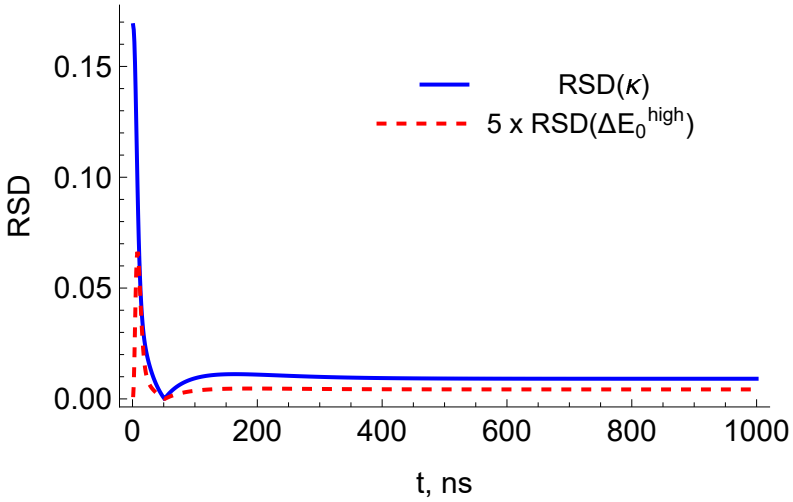


Figure 5. Relative standard deviation of muon transfer time distribution, determined by uncertainties in the initial energy distribution between the two energy components of the muonic hydrogen atoms (solid blue line) and uncertainties in the energy of the high-energy component (dashed red line).

6.4. Uncertainty in $\lambda_{pO}(E)$

Simulations are performed under both moderate and conservative uncertainty scenarios for $\lambda_{pO}(E)$ (see Section 3.8), as depicted in the upper panels of Figure 1. The resulting muon transfer rates are presented in the middle panels of the same figure, with shaded areas representing the standard deviation of $\mathrm{d}N_O/\mathrm{d}t$. The relative standard deviations due to the uncertainties in $\lambda_{pO}(E)$ as functions of time are shown in the bottom panels of Figure 1.

It is evident that the relative 1σ deviations in $RSD(\lambda_{pO})$ induced by the uncertainty in $\lambda_{pO}(E)$ ($\lambda'_{pO}(E)$) for a moderate (conservative) scenario are non-negligible. For times shortly after the formation of $p\mu$ atoms ($0 \div 150$ ns), these deviations reach approximately 15% (80%), and by $t = 1000$ ns, they exceed 70% (80%).

A comparison of the figures indicates that increasing the uncertainty in $\lambda_{pO}(E)$ for $E > 0.1$ eV has minimal impact on the muon transfer rate for times $t \gtrsim 100$ ns. However, during the initial stages of the transfer process, the impact is significant—the relative standard deviation for the two scenarios differs by a factor of five.

Given that the value of $\mathrm{d}N_O/\mathrm{d}t(t)$ decreases exponentially over time, the dominant influence of the uncertainty in $\lambda_{pO}(E)$ on the muon transfer rate is observed at the beginning of the process, specifically for times $t \lesssim 100$ ns, as seen in Figure 1.

6.5. Analytical Considerations

The uncertainty propagation in the muon transfer rate, characterized by its relative standard deviation, can be approximated as

$$RSD(\{X\}) \approx \frac{1}{\mu(\{X\})}\sqrt{\sum_{k=1}^{q}\left(\sigma^{X_k}\frac{\partial}{\partial X_k}\frac{\mathrm{d}N_O}{\mathrm{d}t}(\{\mu^X\})\right)^2}, \quad (10)$$
$$\{X\} = X_1, X_2, \ldots, X_q,\ \{\mu^X\} = \mu^{X_1}, \mu^{X_2}, \ldots, \mu^{X_q},$$

where σ^{X_k} is the standard deviation of X_k, $k = 1, 2, \ldots, q$, and the derivative with respect to X_k is evaluated at the mean values μ^{X_k} of the respective parameters. The derivation of Equation (10) assumes that approximating $\mathrm{d}N_O/\mathrm{d}t(\{X\})$ by a first-order expansion is

valid, and the random variables X_k are statistically independent. From this expression, the general behavior of the relative standard deviation (*RSD*) associated with a given parameter, $RSD(X_k)$, can be qualitatively inferred by considering variations in X_k while keeping the remaining parameters (X_i, $i = 1, \ldots, q$; $i \neq k$) fixed.

The parameters c_O, Λ_{pO}, and $\phi(P/T)$ appear as multiplicative factors of $N(t)$ in the expression (4) for the muon transfer rate from hydrogen to oxygen. Therefore, determining the time of minimum uncertainty, t_0, when any of these parameters is initially uncertain, requires differentiating Equation (4) with respect to time and setting the result equal to zero, which yields the difference in two competing terms that depend on both the initial uncertainty and time. This results in a distinct time of minimum uncertainty, t_0, which differs from the initial time of the process, particularly for the uncertainties associated with c_O, P, T, and Λ_{pO} (Figures 1 and 4). Intuitively, this minimum arises because different contributions to the signal, those affecting the overall normalization and those governing the time evolution, compensate for each other at a specific time, thereby reducing the net sensitivity to variations in the parameter.

Approximate values of the time of minimum uncertainty t_0 in $RSD(X)$, for single parameters $X = c_0,\ P,\ T,\ \Lambda_{pO}$, can be found as a solution of the following equation:

$$\frac{\mathrm{d}N_O}{\mathrm{d}t}(\mu^X + \sigma^X; t_0) - \mu(X; t_0) = 0, \tag{11}$$

where $\mu(X; t_0)$ is the mean muon transfer rate defined in Equation (8). In the general case, the solution of Equation (11) for t_0 and the slopes of $RSD(X)$ at t_0 lack simple closed-form analytical expressions. For that reason, we refrain from presenting overly simplified formulas including linearization of the matrix exponents, though for some specific parameter combinations, this may be attainable.

Parameters such as m_{O_2} and $m_{p\mu}$ (Figure 3), whose uncertainties are incorporated into the aforementioned ones, are not further considered in this context. Additionally, the impact of uncertainties in the initial conditions on the scaling with parameter uncertainties and the time dependence of $RSD(\kappa)$ and $RSD(\Delta E_0^{\mathrm{high}})$ (Figure 5) is not extensively discussed here, as these aspects can be analyzed in a similar manner.

To elucidate some key characteristics of the time-dependent behavior of $RSD(X)$, in the following, we provide specific examples and additional commentary on the $RSD(\{X\})$ time dependence and its scaling with parameter uncertainties.

6.6. Scaling of RSD with Parameter Uncertainties

Expression (10) indicates that, for small deviations of the experimental parameters, the resulting change in $\mathrm{d}N_O/\mathrm{d}t$ must scale nearly linearly with the change in the parameter standard deviation. This assumption was confirmed through numerical simulations. In addition, the uncertainty distribution of $\mathrm{d}N_O/\mathrm{d}t$ was found to be close to normal, except in cases involving very large uncertainties in the model parameters.

6.7. Remarks on the RSD Time Dependence

In the presented simulations, Figures 1, 3, 4 and 6, we observed that, in general, the time behavior of the relative standard deviation defined by various parameters tends to increase at large times. As we have already pointed out, the rate of change of $\mathrm{d}N_O/\mathrm{d}t$ and $RSD(X)$ in time is linear in the first order of approximation, as shown in Figures 3 and 4. This is evident when one considers the exponential time dependence of both $\mathrm{d}N_O/\mathrm{d}t(t)$ and $\mu(t)$ as given by Equations (1) and (4), performs a Taylor expansion in time around $(t - t_0)$ of $(\mathrm{d}N_O/\mathrm{d}t(x_i; t_j) - \mu(X; t_j))$ in the definition of $\sigma(X; t_j)$ (9), and substitutes the result in the definition of $RSD(X)$ (7). However, since the mean value of the muon transfer

rate $dN_O/dt\ \mu(X)$ decreases exponentially with time, the effect of parameter uncertainties on the standard deviation becomes smaller at later times.

As we have already mentioned, for a given combination of experimental parameters, there exists a time interval where the impact of uncertainties in some of the parameters on the relative standard deviation becomes minimal. In the time dependence of RSD due to uncertainties in P, T, c_O, λ_{pO}, a time of minimum uncertainty, t_0, is observed at approximately a few hundred nanoseconds, for the range of change in the mean values of parameters we are interested in. This phenomenon is attributed to faster (slower) $p\mu$ atom depletion in the gas when the particular parameter has a larger (smaller) value.

For instance, this effect is illustrated for a few pressure values in Figure 6. As the pressure P increases from 5 bar to 20 bar, the time corresponding to the lowest RSD shifts from $t_0 \approx 500$ ns to $t_0 \approx 150$ ns. A similar trend is observed for other parameters, reflecting the underlying relationship between these parameters and the muon transfer rate dN_O/dt, as described by Equations (1) and (2).

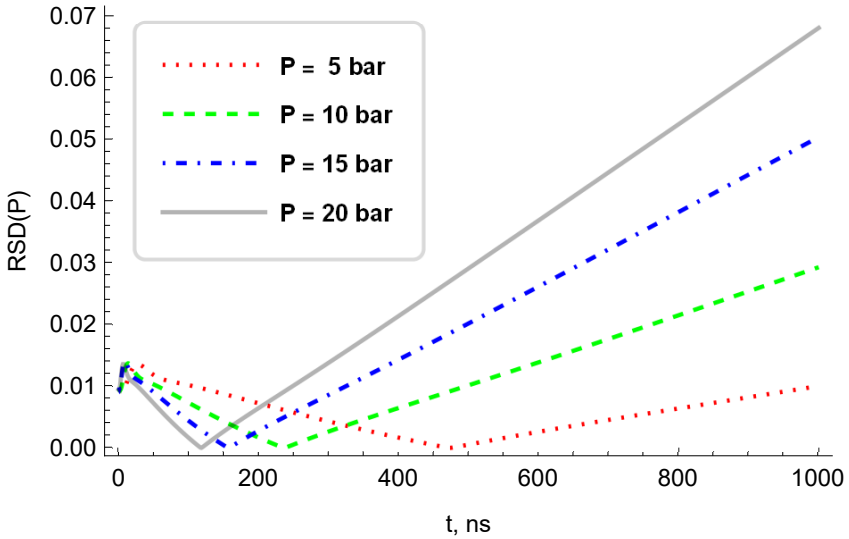


Figure 6. Relative standard deviation of the muon transfer rate due to uncertainties in pressure for four different mean values of its distribution. The dotted red, dashed green, dot-dashed blue and solid gray lines correspond to mean values of $P = 5, 10, 15$ and 20 bar, respectively. In all cases, the pressure uncertainty is 1%.

This effect has several potential applications. For instance, identifying the time interval of low RSD allows for improved comparison of results between experiments and/or numerical simulations. For a specific experiment, it can also assist in calibration processes. Moreover, by optimizing the experimental parameters to exploit this effect, it may be possible to enhance the precision of the measurements, potentially by reducing the impact of parameter uncertainties during the critical interval of observation.

7. Self-Consistency Check of the Proposed Model with a Two-Step Muon Transfer Rate Fitted to Experimental Data

To validate the underlying principles and assumptions of the proposed model introduced in Section 2 (Equations (1)–(4)), we compare its predictions with the experimental data reported in Ref. [11]. In order to isolate the impact of the energy-dependent muon transfer rate $\lambda_{pO}(E)$—which introduces significant uncertainty in our simulations—we employ a simplified two-step muon transfer rate function $\lambda^W_{pO}(E)$, obtained in Ref. [11] by fitting to experimental data:

$$\lambda_{pO}^{W}(E) = \begin{cases} 0.85 \times 10^{11}, & 0 \text{ eV} < E \leq 0.12 \text{ eV}, \\ 2.08 \times 10^{11}, & 0.12 \text{ eV} < E \leq 0.22 \text{ eV}, \\ 0, & \text{otherwise.} \end{cases} \quad (12)$$

Although this parametrization is not physically motivated, it provides a useful benchmark for assessing the internal consistency of the proposed model. Since both the experimental data and the corresponding two-step transfer rate function $\lambda_{pO}^{W}(E)$ originate from the same work [11], this comparison effectively constitutes a self-consistency check. In particular, if the present model is adequate, the use of $\lambda_{pO}^{W}(E)$ as input should reproduce results in close agreement with the experimental data from which it was originally derived.

The function $\lambda_{pO}^{W}(E)$ is shown in Figure 7a by the dashed red line, while the muon transfer rate $\lambda_{pO}(E)$ extracted from the FAMU experiment [13] is shown by the solid blue line. In this comparison, we do not attempt to estimate the uncertainty of $\lambda_{pO}(E)$ for $E > 0.1$ eV; instead, we display only the 95% confidence interval up to $E = 0.1$ eV, as reported in Ref. [13] (shaded region). The zero transfer rate is indicated by the dash-dotted line. A notable difference between the two functions is observed: the two-step model underestimates the muon transfer rate for $E < 0.1$ eV, while suggesting larger values at higher energies.

We simulate the time dependence of the characteristic X-ray emission rate using $\lambda_{pO}^{W}(E)$, while keeping all other parameters fixed as specified in Section 3. The results are shown in Figure 7b (dashed red line). A very good agreement with the experimental data (green "+" symbols) is observed. The simulated and experimental results are consistent both at early times ($t < 100$ ns) and at later times. This agreement not only supports the reliability of the proposed model but, in combination with observations from Figure 7a, also suggests that further investigation of the energy dependence of the muon transfer rate to oxygen is necessary, particularly for $E > 0.1$ eV, where the current uncertainty remains significant.

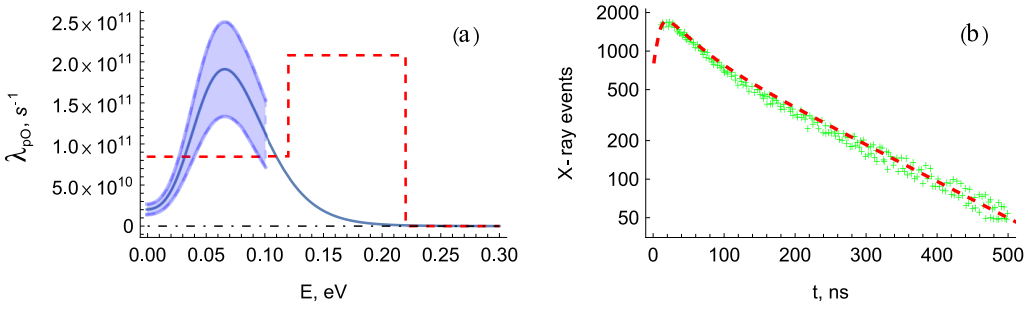


Figure 7. (**a**) The dashed red line represents the two-step muon transfer rate $\lambda_{pO}^{W}(E)$ defined in Equation (12). For comparison, the muon transfer rate $\lambda_{pO}(E)$, with its 95% confidence interval (shadowed area), from [13], used throughout this work, is shown by the solid blue line. (**b**) The X-ray emission event rate obtained using the simplified two-step function $\lambda_{pO}^{W}(E)$ is shown by the dashed red line. The experimental data are indicated by green "+" symbols.

The physical interpretation of the elevated X-ray emission rate observed during the first tens of nanoseconds when the two-step transfer rate $\lambda_{pO}^{W}(E)$ is used is as follows: For the range of parameter values considered, the thermalization of the $p\mu$ atoms occurs within approximately 10–20 ns. However, the simulations indicate that, up to about 100 ns, a non-negligible population of epithermal $p\mu$ atoms with energies in the range 0.1–0.3 eV persists. Since the function $\lambda_{pO}^{W}(E)$ attains relatively large values in this energy range, it leads to an enhanced muon transfer rate to oxygen and, consequently, to increased X-ray emission. At later times ($t > 100$ ns), the epithermal $p\mu$ population is largely depleted due to ongoing thermalization and transfer processes, and only the low-energy region

($E < 0.1$ eV) contributes significantly. In this regime, both $\lambda_{pO}^{W}(E)$ and $\lambda_{pO}(E)$ yield similar behavior for the X-ray emission rate.

8. Simulations and Comparison with Experimental Data

In the previous section, we validated the proposed model's predictability and self-consistency with a simplified two-step muon transfer function. Here, we will apply it to a real-world scenario by simulating the muon transfer rate from hydrogen to oxygen using the full set of model parameters as specified in Section 3. In order to test the precision and accuracy of our model versus a real-world scenario, we simulated the muon transfer rate from hydrogen to oxygen using the experimental parameters from [11] as specified in Section 3. In line with the analysis in Sections 5 and 6, we account for the uncertainties in the parameters that have the most significant impact on the simulation precision—namely, the pressure P and temperature T of the gas mixture, the oxygen concentration c_O, the initial distribution of μp, and the transfer rate of muons to oxygen, λ_{pO}. This approach allows for a Monte Carlo simulation that more densely traverses the parameter space. The simulation results showing the transfer rates from hydrogen to oxygen as a function of time along with their corresponding standard deviation are plotted alongside the experimental data from Werthmüller et al. [11] in Figure 8.

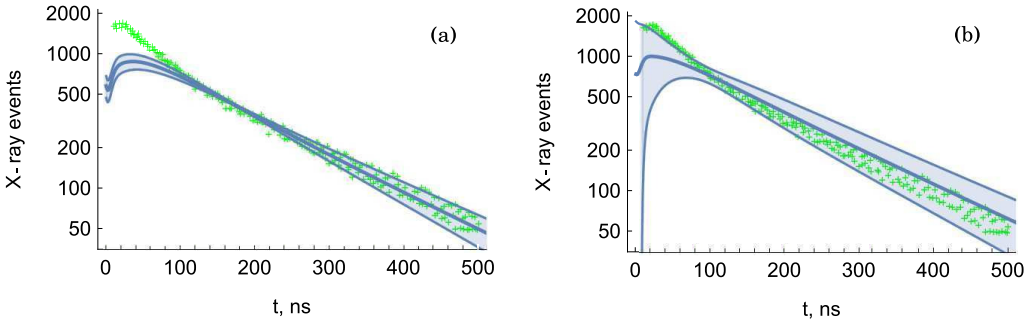


Figure 8. Simulations of the X-ray emission event rate (solid purple-blue line) alongside measured data from [11] (green "+" symbols). The thick solid purple-blue line represents the mean of all computed curves $\mathrm{d}N_O/\mathrm{d}t$ on a logarithmic scale, while the shadowed area denotes the 1σ standard deviation due to parameter uncertainties. The left (**a**) and right (**b**) panels correspond to the moderate and conservative scenarios for the energy-dependent muon transfer rate to oxygen, λ_{pO} and λ'_{pO}, as shown in Figure 1, respectively.

The simulations incorporate the transfer rate $\lambda_{pO}(E)$ from [13], using both moderate and conservative scenarios for its uncertainty, as shown in Figure 1. The results for these scenarios are displayed in the left and right panels of Figure 8, respectively. The measured X-ray event rates are expected to be proportional to the muon transfer rate on a logarithmic scale, with the scaling factor depending on specific experimental factors, such as detector efficiencies, the number of observed characteristic frequencies, the initial population of $p\mu$ atoms in the target, and more. This scaling factor is determined by matching the average value of $\mathrm{d}N_O/\mathrm{d}t$ from the simulation to the experimental data fit at $t = 170$ ns for λ_{pO} and at 110 ns for λ'_{pO}, as these times correspond to periods where the relative standard uncertainty in the muon transfer event rate is approximately minimal.

It is worth noting that in the full Monte Carlo simulation, where the uncertainties of multiple parameters are taken into account, a distinct time at which the overall uncertainty reaches a minimum is observed (visible in both panels of Figure 8). This indicates that such a feature is also preserved in simulations involving multiple parameters. This behavior may have practical implications for more realistic calibration and optimization of muon experiments as a whole.

Figure 8 shows a very good agreement between the simulation and the experiment at times $t \gtrsim 150$ ns. However, a notable discrepancy in the slope of the emission event rate is observed for $t \lesssim 100$ ns. The discrepancy results in a slight upward shift in the simulated curve relative to the experimental data for $t \gtrsim 150$ ns in Figure 8b, as the matching is performed at a time when the experimental behavior deviates from the expectations. This deviation is challenging to explain solely through the uncertainties in the physical constants (Table 1) or the experimental parameters (Table 2).

Several factors may contribute to this discrepancy. For instance, our approximation of the initial $p\mu$ distribution as a "two-component" model, based on experimental [11] and theoretical studies [23], may be too simplistic. However, it could partly explain the discrepancy as the uncertainties stemming from this approximations could be significant in the first tens of nanoseconds, as can be seen in Figure 5. The same reasoning applies to the neglected time dependence of Λ_{pO} and to the unknown transfer rate to oxygen from the $p\mu$ triplet state (see Section 3.8); their influence on the emitted radiation persists only until thermalization is achieved. Another potential reason is the lack of a reliable expression for the energy-dependent muon transfer rate $\lambda_{pO}(E)$, for energies E higher than 0.1 eV. In this case, we have to assume that the uncertainty in $\lambda_{pO}(E)$ is larger for $E > 0.1$ eV. When the conservative uncertainty estimate is used, all experimental data points fall within or very close to the 1σ uncertainty band, as shown in Figure 8b.

Our observations and those in [11] suggest that the energy-dependent muon transfer rate $\lambda_{pO}(E)$ for $E > 0.1$ eV could be higher than currently assumed. The higher values of $\lambda_{pO}(E)$ at elevated energies lead not only to faster but also to more prolonged and deeper depletion of high-energy muonic hydrogen in the gas mixture, which may account for the observed discrepancy. This is further supported by Werthmüller et al. [11], who show that a specific functional dependence of $\lambda_{pO}(E)$ can be constructed to reproduce the experimental results (see Section 7). The physical origin of such heightened values of $\lambda_{pO}(E)$ may be attributed to effects arising from the internal structure of O_2 and $p\mu$. Investigation of this hypothesis would require a dedicated study. In principle, the value of $\lambda_{pO}(E)$ could be tested through an experiment designed to measure the muon transfer rate as a function of the collision energy, with high resolution, during the first tens of nanoseconds after $p\mu$ formation, until the system is in a non-stationary state.

9. Conclusions

We study the characteristic time-dependent X-ray emission resulting from muon transitions to the lower-energy states in oxygen after their transfer from muonic hydrogen. In the developed model, the kinetic energy and spin distribution of $p\mu$ atoms is evolved in time by accounting for the possible channels that alter their state. The decay and scattering of muonic hydrogen, as well as its probability of transferring to another constituent of the surrounding medium, are modeled by using the relevant transition rate matrix. The impact of the uncertainties in the experimental parameters is investigated by means of the Monte Carlo method, and the main sources of uncertainty are identified. The results obtained from the proposed model are in good agreement with the available experimental data, especially at relatively long times. However, within the first hundred nanoseconds, there is a discrepancy that may be due to an unaccounted effect or inaccuracies in the rates used. Thus, the model provides a realistic description of processes involving muonic hydrogen, while different sources of uncertainty are assessed. Moreover, the presence of a minimum in the relative standard deviation can serve as a benchmark for comparing experiments and numerical simulations, aid in calibration processes, and enhance measurement precision by minimizing the impact of parameter uncertainties during the observation period. These

results could be useful and may find application in the planning and analysis of both current and future muonic experiments.

Author Contributions: Conceptualization, I.B.; Methodology, P.D.; Software, P.D., I.B. and H.T.; Validation, H.T. and I.B.; Formal analysis, I.B.; Investigation, I.B. and P.D.; Data curation, P.D.; Writing—original draft preparation, P.D.; Writing—review and editing, I.B. and H.T.; Visualization, P.D. and H.T.; Supervision, H.T.; Project administration, I.B. All authors have read and agreed to the published version of the manuscript.

Funding: This research was funded by Bulgarian Science Fund grant number KP-06-N58/5 from 19 November 2021.

Data Availability Statement: The datasets generated during and analyzed during the current study are available from the corresponding authors (petar_danev@abv.bg, borajiev@inrne.bas.bg) on reasonable request.

Acknowledgments: This work was supported by the Bulgarian Science Fund under contract KP-06-N58/5 from 19 November 2021. The authors would like to express their gratitude to A. Adamczak for providing the muonic hydrogen scattering rates. During the preparation of this work, the authors used ChatGPT-4 in order to improve the readability and language of the manuscript. After using this tool, the authors reviewed and edited the content as needed and take full responsibility for the content of the published article.

Conflicts of Interest: The authors declare no conflicts of interest.

Abbreviations

The following abbreviations are used in this manuscript:

LHD	Liquid hydrogen density
RSD	Relative standard deviation

References

1. Schenkel, M.R.; Alighanbari, S.; Schiller, S. Laser spectroscopy of a rovibrational transition in the molecular hydrogen ion. *Nat. Phys.* **2024**, *20*, 383–388. [CrossRef]
2. Alighanbari, S.; Giri, G.S.; Constantin, F.L.; Korobov, V.I.; Schiller, S. Precise test of quantum electrodynamics and determination of fundamental constants with HD^+ ions. *Nature* **2020**, *581*, 152–158. [CrossRef] [PubMed]
3. Pohl, R.; Antognini, A.; Nez, F.; Amaro, F.D.; Biraben, F.; Cardoso, J.M. The size of the proton. *Nature* **2010**, *466*, 213–216. [CrossRef] [PubMed]
4. Dupays, A.; Beswick, A.; Lepetit, B.; Rizzo, C.; Bakalov, D. Proton Zemach radius from measurements of the hyperfine splitting of hydrogen and muonic hydrogen. *Phys. Rev. A* **2003**, *68*, 052502. [CrossRef]
5. Volotka, A.V.; Shabaev, V.M.; Plunien, G.; Soff, G. Zemach and magnetic radius of the proton from the hyperfine splitting in hydrogen. *Eur. Phys. J. D* **2005**, *33*, 23–27. [CrossRef]
6. Antognini, A.; Nez, F.; Schuhmann, K.; Amaro, F.D.; Biraben, F.; Cardoso, J.M.; Covita, D.S.; Dax, A.; Dhawan, S.; Diepold, M.; et al. Proton structure from the measurement of 2S-2P transition frequencies of muonic hydrogen. *Science* **2013**, *339*, 417–420. [CrossRef]
7. Djukanovic, D.; Djukanovic, D.; von Hippel, G.; Meyer, H.B.; Ottnad, K.; Salg, M.; Wittig, H. Zemach and Friar radii of the proton and neutron from lattice QCD. *Phys. Rev. D* **2024**, *110*, L011503. [CrossRef]
8. Ruth, D.; Slifer, K.; Chen, J.P.; Carlson, C.E.; Hagelstein, F.; Pascalutsa, V.; Deur, A.; Kuhn, S.; Ripani, M.; Zheng, X.; et al. New Spin Structure Constraints on Hyperfine Splitting and Proton Zemach Radius. *Phys. Lett. B* **2024**, *859*, 139116. [CrossRef]
9. Antognini, A.; Hagelstein, F.; Pascalutsa, V. The Proton Structure in and out of Muonic Hydrogen. *Ann. Rev. Nucl. Part.* **2022**, *72*, 389–418. [CrossRef]
10. Pizzolotto, C.; Adamczak, A.; Bakalov, D.; Baldazzi, G.; Baruzzo, M.; Benocci, R.; Bertoni, R.; Bonesini, M.; Bonvicini, V.; Cabrera, H.; et al. The FAMU experiment: Muonic hydrogen high precision spectroscopy studies. *Eur. Phys. J. A* **2020**, *56*, 185. [CrossRef]
11. Werthmüller, A.; Adamczak, A.; Jacot-Guillarmod, R.; Mulhauser, F.; Schaller, L.A.; Schellenberg, L.; Schneuwly, H.; Thalmann, Y.-A.; Tresch, S. Energy dependence of the charge exchange reaction from muonic hydrogen to oxygen. *Hyperfine Interact* **1998**, *116*, 1–16. [CrossRef]
12. Mulhauser, F.; Schneuwly, H. Muon transfer to sulphur dioxide. *J. Phys. B* **1993**, *26*, 4307. [CrossRef]

13. Stoilov, M.; Adamczak, A.; Bakalov, D.; Danev, P.; Mocchiutti, E.; Pizzolotto, C.; Baldazzi, G.; Baruzzo, M.; Benocci, R.; Bonesini, M.; et al. Experimental determination of the energy dependence of the rate of the muon transfer reaction from muonic hydrogen to oxygen for collision energies up to 0.1 eV. *Phys. Rev. A* **2023**, *107*, 032823. [CrossRef]
14. Pizzolotto, C.; Sbrizzi, A.; Adamczak, A.; Bakalov, D.; Baldazzi, G.; Baruzzo, M.; Cabrera, H.; Cirrincione, D.; Clemenza, M.; Colace, L.; et al. Measurement of the muon transfer rate from muonic hydrogen to oxygen in the range 70–336 K. *Phys. Lett. A* **2021**, *403*, 127401. [CrossRef]
15. Adamczak, A. Differential cross sections for muonic atom scattering from hydrogenic molecules. *Phys. Rev. A* **2006**, *74*, 042718. [CrossRef]
16. Mocchiutti, E.; Adamczak, A.; Bakalov, D.; Baldazzi, G.; Benocci, R.; Bertoni, R.; Bonesini, M.; Bonvicini, V.; Cabrera Morales, H.; Chignoli, F.; et al. First measurement of the temperature dependence of muon transfer rate from muonic hydrogen atoms to oxygen. *Phys. Lett. A* **2020**, *384*, 126667. [CrossRef]
17. Nuber, J.; Adamczak, A.; Abdou Ahmed, M.; Affolter, L.; Amaro, F.D.; Amaro, P.; Antognini, A.; Carvalho, A.; Chang, Y.-H.; Chen, T.-L.; et al. Diffusion of muonic hydrogen in hydrogen gas and the measurement of the 1s hyperfine splitting of muonic hydrogen. *SciPost Phys. Core* **2023**, *6*, 057. [CrossRef]
18. Measday, D.F. The nuclear physics of muon capture. *Phys. Rep.* **2001**, *354*, 243–409. [CrossRef]
19. Mocchiutti, E.; Bonvicini, V.; Carbone, R.; Danailov, M.; Furlanetto, E.; Gadedjisso-Tossou, K.S.; Guffanti, C.; Pizzolotto, A.; Rachevski, L.; Stoychev, E.; et al. First FAMU observation of muon transfer from μp atoms to higher-Z elements. *J. Instrum.* **2018**, *13*, P02019. [CrossRef]
20. Andreev, V.A.; Banks, T.I.; Carey, R.M.; Case, T.A.; Clayton, S.M.; Crowe, K.M. Measurement of the Formation Rate of Muonic Hydrogen Molecules. *Phys. Rev. C* **2015**, *91*, 055502. [CrossRef]
21. Mohr, P.; Newell, D.; Taylor, B.; Tiesinga, E. CODATA Recommended Values of the Fundamental Physical Constants: 2022. *Rev. Mod. Phys.* **2025**, *97*, 025002. [CrossRef]
22. The Engineering ToolBox. Hydrogen—Density and Specific Weight vs. Temperature and Pressure. Available online: https://www.engineeringtoolbox.com/hydrogen-H2-density-specific-weight-temperature-pressure-d_2044.html (accessed on 1 April 2026).
23. Markushin, V.E. Atomic cascade in muonic hydrogen and the problem of kinetic-energy distribution in the ground state. *Phys. Rev. A* **1994**, *50*, 1137. [CrossRef]
24. Duman, E.L.; Men'shikov, L.I.; Smirnov, B.M. Exchange reaction of an atom with a multiply charged ion. *Sov. Phys. JETP* **1979**, *50*, 433.

Disclaimer/Publisher's Note: The statements, opinions and data contained in all publications are solely those of the individual author(s) and contributor(s) and not of MDPI and/or the editor(s). MDPI and/or the editor(s) disclaim responsibility for any injury to people or property resulting from any ideas, methods, instructions or products referred to in the content.